

pubs.acs.org/estengg Article

Evaluating Long-Term Treatment Performance and Cost of Nutrient Removal at Water Resource Recovery Facilities under Stochastic Influent Characteristics Using Artificial Neural Networks as Surrogates for Plantwide Modeling

Shaobin Li, Seyed Aryan Emaminejad, Samuel Aguiar, Aliza Furneaux, Ximing Cai, and Roland D. Cusick



Cite This: ACS EST Engg. 2021, 1, 1517–1529



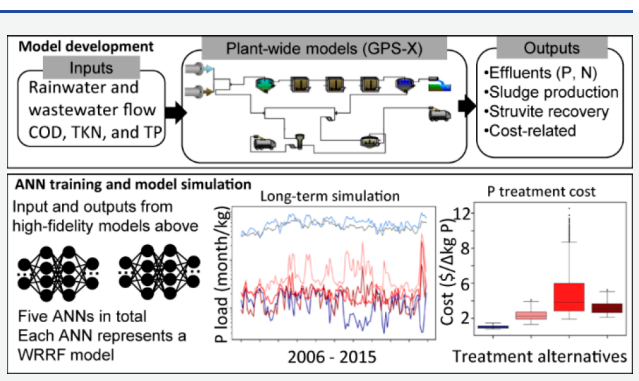
ACCESS

III Metrics & More

Article Recommendations

s Supporting Information

ABSTRACT: Integrated watershed modeling is needed to couple water resource recovery facilities (WRRFs) with agricultural management for holistic watershed nutrient management. Surrogate modeling can facilitate model coupling. This study applies artificial neural networks (ANNs) as surrogate models for WRRF models to efficiently evaluate the long-term treatment performance and cost under influent fluctuations. Specifically, we first developed five WRRFs, including activated sludge, activated sludge with chemical precipitation (ASCP), enhanced biological phosphorus removal (EBPR), EBPR with acetate addition (EBPR-A), and EBPR with struvite recovery (EBPR-S), in a high-fidelity simulation program (GPS-X). The five WRRFs were based on an existing plant that treats combined domestic and industrial wastewater. The ANNs



have satisfactory performance in capturing nonlinear biological behaviors for all five WRRFs, even though the prediction performance (*R*-square) slightly decreases as the model complexity increases. We advanced ANNs application in WRRF models by simulating long-term (10-yr) performance with monthly influent fluctuations using ANNs trained by simulation data from steady-state models and evaluated their performance on Phosphorus (P) and Nitrogen (N) removal. EBPR-S shows the most resilience, while EBPR is more sensitive to influent characteristics impacted by stormwater inflow. When comparing life cycle costs of N and P removal for each layout over the 10-yr simulation period, EPBR-S is the most cost-effective alternative, highlighting both the operational and cost benefits of side-stream P recovery. By capturing both nonlinear behaviors of biological treatment and operating costs with computationally lean ANNs, this study provides a paradigm for integrating complex WRRF models within integrated watershed modeling frameworks.

KEYWORDS: nutrient removal, machine learning, Bardenpho enhanced biological phosphorus removal, phosphorus recovery, techno-economic analysis

1. INTRODUCTION

Nitrogen and phosphorus pollution from urban and industrial point sources, and agricultural nonpoint sources are the major contributors to harmful algal blooms and hypoxia in both critical drinking water resources and saltwater ecosystems. ^{1–3} This phenomenon is especially detrimental to aquatic organisms that cannot tolerate low dissolved oxygen levels (generally below 2 mg/L), as is the case of the hypoxic zone in the Gulf of Mexico, ³ which covered 5480 km² in 2020. ⁴ In response to the 2018 Gulf Hypoxia Action Plan by the federal Environmental Protection Agency, the Illinois Environmental Protection Agency (IEPA) initiated the Illinois Nutrient Loss Reduction Strategy (NLRS) to reduce 45% of the nitrogen and phosphorus load by 2045. ⁵ To achieve the nutrient reduction goal outlined in the NLRS, considerable changes to both

nonpoint (e.g., agricultural runoff) and point source (waste-water treatment effluent) management are needed. For nonpoint sources, nutrient pollution can be reduced by adopting various agricultural best management practices.^{6,7} For point sources, nutrient pollution can be reduced by optimizing the existing wastewater treatment and resource recovery processes used in water resource recovery facilities

Received: May 17, 2021 Revised: August 26, 2021 Accepted: August 27, 2021 Published: September 9, 2021





(WRRFs) or upgrading to a more advanced treatment process with new infrastructure.^{8,9} Integrated models that simulate the effectiveness of point source and nonpoint source nutrient reductions are required for holistic nutrient management at watershed scales.^{10,11}

Various computer programs (e.g., GPS-X and BioWin) have been developed that allow for simulation of WRRF treatment alternatives. f2-15 In practice, these simulators help identify alternative processes that best align with point source nutrient reduction goals and determine the most cost-effective approaches to nutrient reduction. These types of simulations also allow for scenario-based experimentation without disturbing a real WRRF's operation. However, integration of a point source model with other nonpoint source models for system-based solutions to watershed optimization studies are challenging, as process modeling software are typically proprietary and do not natively integrate with external programs. Though some software have recently begun providing application programming interface (API) to enable integration, they usually come with the requirement of a commercial license to use their API. Integrating models with commercial license requirements discourages modelers as such requirements would make the developed models less likely to be transferred and reused by others. Moreover, the computation time for such API-connected integrated models can be expensive. Developing ANN-based WRRF surrogate models can facilitate the integration of WRRF models with other models on the same platform. In another work that focused on model integration coupling multiple process and empirical models, we demonstrated the importance of surrogating a process model to facilitate model integration. WRRF plant-wide models can also be computationally expensive to execute, depending on the degree of complexity for various treatment processes (e.g., activated sludge versus enhanced biological phosphorus removal), number of simulations required, and temporal scales (e.g., real-time, daily, monthly, annual).16 By developing data-driven WRRF surrogate models, wastewater treatment performance under various combinations of influent characterisitics and fluctuations can be evaluated efficiently, instead of using processbased WRRF models in a commercial software package to run the simulation. Therefore, different variants of surrogate models (also called emulators, data-driven models, etc.) have been applied and are needed to approximate the nonlinear behaviors of process-based models with efficient computation time while maintaining satisfactory performance.

Among various surrogate models, artificial neural networks (ANNs) have grown in popularity with promising applications for which a high degree of nonlinearity exists within a data set. 17-20 ANNs have also shown to be capable of predicting WRRF treatment performance in various settings. 21-27 In some applications, historical WRRF operational data are used to train and test ANNs; while this method can accurately reflect the process operation, ANNs directly trained with historical data cannot compare proposed treatment process scenarios for nutrient removal and recovery. In addition, the sizes of data sets are usually limited (e.g., less than 100 data points) and can result in overfitting issues. 22,27 Another limitation in the literature derives from ANNs trained solely with simulated data based on the activated sludge models (ASMs) with simple process layouts.^{25,26} Moreover, simulating the long-term dynamic treatment performance of WRRFs is challenging because of the lack of detailed knowledge of

influent wastewater characteristics and how rainfall events would translate to plant influent and operational changes (e.g., sludge wastage, airflow, recycle rate, etc.) over the long-term. Therefore, further investigation into how ANNs perform when they are used to predict the performance of complex process layouts and nutrient recovery scenarios are needed.

To address these limitations, the objective of this work is to develop different numerical process models based on the operation of an existing plant and apply Monte Carlo sampling to generate sufficient training data sets that represent various influent compositions for ANN model training. The trained ANN models were then used to compare the long-term performance of multiple plant layouts using several years of historical monthly data. We also used ANNs to estimate costs based on predictions for certain operational variables (e.g., airflow demand, biosolids production, chemical consumption). We then compared the life cycle costs of treatment alternatives for nutrient removal and recovery under various influent compositions and wet weather conditions. The surrogate models developed in this work have been further coupled with other nonpoint source hydrological models for integrated technology-environment-economics modeling (ITEEM), which is part of a separate work focused on surrogate-based model coupling.11

2. METHODOLOGY

We first developed five steady-state WRRF treatment alternatives in GPS-X (Hydromantis, Inc.) under stochastic influent characteristics (10 000 random combinations of influent characteristics within their ranges). The first WRRF model was an activated sludge (AS) process that served as the baseline treatment level and was designed to mirror the existing WRRF in our test watershed. The modeling accuracy was assessed by comparing the AS simulation results to historical data obtained from a similar process used in a WRRF located in Illinois, USA.

The operating conditions and unit processes' dimensions/ capacities used in the model were matched with the real WRRF to ensure the GPS-X model was calibrated to the characteristics of the plant. The operating conditions included mainline treatment SRT and HRT, DO values in aeration basins, anaerobic digestion unit residence time, primary and secondary clarification capacity, and underflow solids concentration in the sludge thickening unit. The steady-state WRRF model was further calibrated to the average effluent nitrate and TP concentrations of the plant's historical data (see Figure 2a,c). The current calibration approach had a limitation as it was not calibrated to the dynamic effluent data of the plant using a dynamic mode; however, calibrating a WRRF model over a long-term period in a dynamic mode could be very challenging as the plant had undergone various operational changes over time that could significantly impact the plant's treatment performance.

Furthermore, partial denitrification was implemented in the simulations to match the process with the existing WRRF. The other four WRRF treatment alternatives included additional chemical and biological nutrient removal (BNR) processes. We then cleaned the simulation data by removing runs that had failed to converge on a steady state solution. ANNs were subsequently applied to surrogate the five WRRF treatment alternatives with different degrees of complexity.

The developed ANNs predicted the effluent nutrient concentrations and other operational data, such as aeration

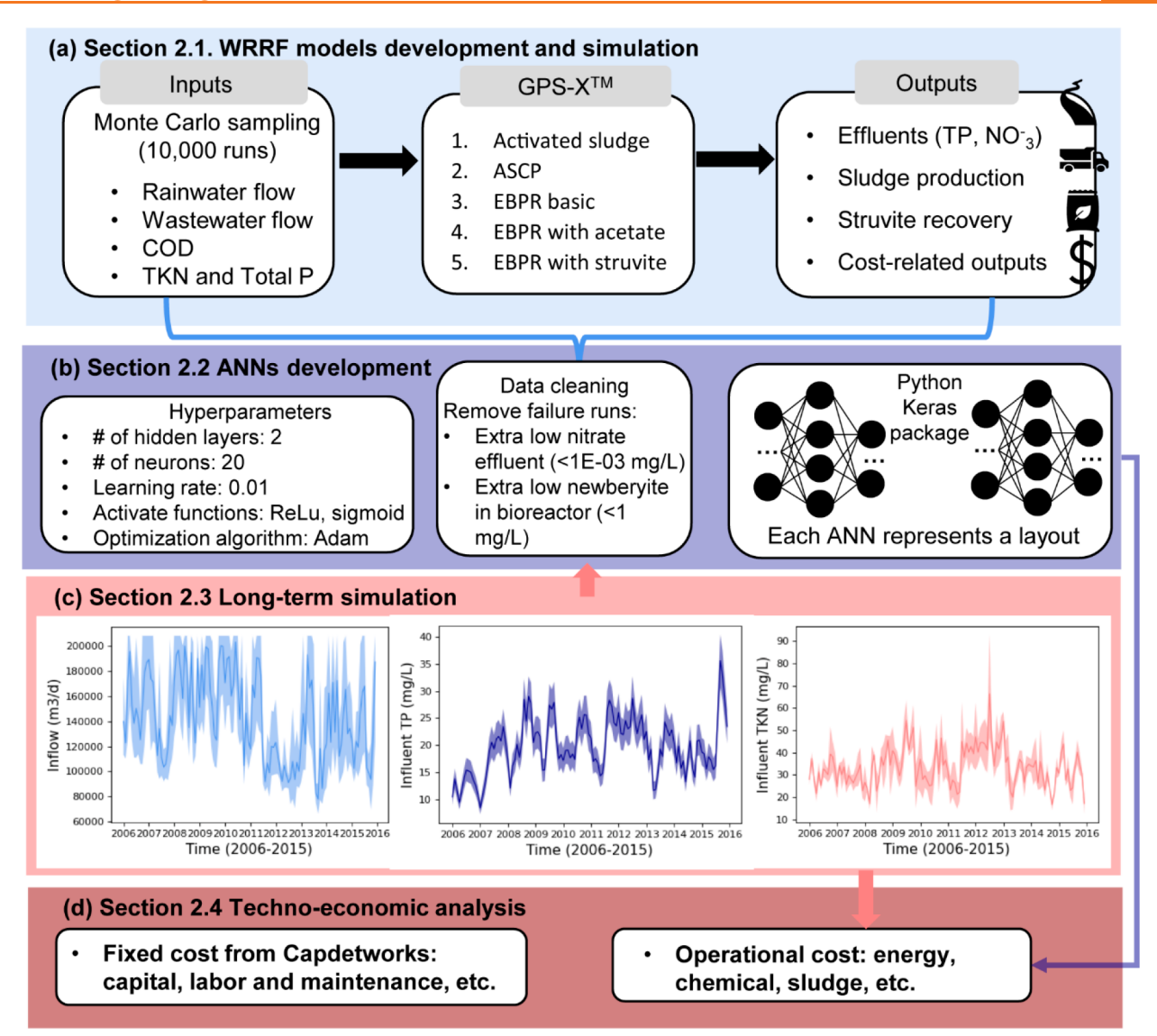


Figure 1. Schematic workflow of this study: Section 2.1, developing WRRF models in GPS-X simulation software (a); section 2.2, ANNs development (b); section 2.3, long-term simulation (c); section 2.4, techno-economic analysis of WRRF models (d).

requirements, sludge production, chemical use, and fertilizer recovery potential, which were further used to conduct a techno-economic analysis (TEA) of nutrient removal and recovery potential for the five WRRF alternatives. After the ANNs were successfully developed and validated, we compared the nutrient treatment performance and cost effectiveness among the five WRRF treatment alternatives for 10 years (2006–2015) of historical influent conditions. The overall workflow of this study is provided in Figure 1.

- **2.1. Plantwide Modeling of Five WRRF Treatment Alternatives.** In this section, we present the details of plantwide modeling development for the five WRRF treatment alternatives as well as the design space for characterizing stochastic influent characteristics, including wastewater flow, rainwater flow, total phosphorus (TP), total Kjeldahl nitrogen (TKN), and chemical oxygen demand (COD).
- 2.1.1. Plant Layout Design for WRRF Treatment Alternatives. The plant-wide models provided a comparison of the effectiveness of plant configurations in P removal and potential phosphorus recovery as struvite. Full-scale WRRFs were modeled and simulated using GPS-X software from

Hydromantis, Inc. for an existing WRRF located in Central Illinois. The WRRF receives high strength nutrient influents from various industrial users and has a design average flow rate of 41 million gallons per day (MGD) with a design maximum flow of 125 MGD. The plant currently operates with an activated sludge treatment process to meet numeric criteria for total suspended solids (TSS), biochemical oxygen demand (BOD), and ammonia and anticipates a future total P discharge limit of 1 mg-P L-1. The nutrient removal configurations considered are activated sludge (AS), activated sludge with ferric chloride chemical precipitation for P removal (ASCP), modified Bardenpho enhanced biological phosphorus removal (EBPR), EBPR with acetate addition (EBPR-A), and EBPR with side-stream struvite precipitation (EBPR-S). As one of the modeling goals was to achieve minimum nutrient effluent concentrations, we also applied the built-in optimization tools of GPS-X to each treatment alternative.

In the AS and ASCP GPS-X process layouts (Supporting Information, Figure S1a,b), influent wastewater flow and rainwater were mixed before being directed to a primary clarifier unit, followed by aeration tanks (three reactors in

series). The chemical (FeCl₃) in the ASCP process was added based on a 1:1 molar ratio between Fe³⁺ and influent PO₄^{3-.28} A diffused aeration system was used in the aeration tanks with dissolved oxygen (DO) set points of 0.5, 2.3, and 3.3 mg O_2/L in reactors 1 to 3 in accordance with current operations at the plant. Two secondary clarifier units were used in series, before the disinfection unit. Part of the underflow from the secondary clarifiers was directed back to mainline treatment, and part of it was directed to solids handling unit processes as wasted sludge. Wasted sludge combined with the primary clarifier underflow entered a sludge thickening unit, followed by anaerobic digestion. The digestion unit effluent was directed to a dewatering unit, where the dewatered sludge was hauled out of the treatment plant, and its effluent was returned to mainline treatment. The ASCP layout had a FeCl3 chemical addition tank upstream of the secondary clarifiers.

In the EBPR layout (Figure S1c), the effluent of the primary clarifier unit (same as AS and ASCP) was directed to biological treatment basins. The acetate dosing tank was off-line in this process, and biological treatment basins consisted of one anaerobic tank, two anoxic tanks, and two aeration tanks. The combined flow of wasted activated sludge and primary clarifier underflow were directed to thickening and digestion units operated under the same conditions as the AS and ASCP processes. A centrifuge was used for dewatering the sludge (removal efficiency of particulate inert material = 0.95), with dewatered sludge being hauled, and the effluent directed back to headworks. The EBPR-A layout had the acetate dosing tank operational, upstream of the anaerobic tank, where acetate was added to maintain a COD/TP ratio of 26-30 based on influent concentrations. In the EBPR-S process (Figure S1d), the effluent of the centrifuge was not directed back to the headworks, instead, it was mixed with MgCl₂ and NaOH before entering the fluidized bed reactor. MgCl2 was added based on a molar ratio of 1.3 between Mg²⁺ and PO₄³⁻, and NaOH was added to have a 1:1 molar ratio with Mg²⁺. 28 Struvite pellets were collected from the bottom of the reactor, and the reactor effluent was directed back to headworks. Unit process dimensions are presented in SI Tables S1 and S2.

2.1.2. Design Space for Characterizing Stochastic Influents. Once the plantwide models were developed, we generated the stochastic influent characteristics to represent the intrinsic variability of sewage characteristics and wet weather. The influent characteristics (e.g., wastewater flow, rainwater flow, COD, TP, TKN) were obtained from the existing WRRF and their ranges are provided in Table 1. For the intrinsic variability of sewage characteristics, we used maximum and minimum influent characteristics (e.g., COD, TP, TKN) reported by the WRRF as the range to uniformly sample data. The uniform distributions were selected to evenly span samples across the parameter space and facilitate ANNs

Table 1. Characterization of Stochastic Influent for the WRRF to Generate Dataset for ANN Training and Testing

influent characteristics	range	unit	distribution
influent flow	20-55	MGD (US)	uniform
wastewater flow	20-30	MGD (US)	
rainwater flow	30-55	MGD (US)	
total phosphorus (TP)	11.0-38.9	$mg-P L^{-1}$	uniform
total Kjeldahl nitrogen (TKN)	14.6-49.4	mg-N L ⁻¹	uniform
chemical oxygen demand (COD)	447-752	$mg L^{-1}$	uniform

learning of nonlinear behavior across a wide range of parameter space. The influent flow, including wastewater and rainwater flow, was uniformly sampled between 20 and 55 MGD to reflect the variability of wet weather. On the basis of personal communication with the plant operator, the inflow lower than 30 MGD was considered as only wastewater flow from sanitary sewage (e.g., domestic and industrial), while any flow exceeding 30 MGD was attributed to rainwater to account for its dilution impact on influent concentration. Typical values of rainwater characteristics (e.g., COD, TP, TN) from the literature were used to account for pollutant loadings in combined influents.²⁹ Monte Carlo methods were used to uniformly generate 10 000 sampled influent characteristics (i.e., flow rate, total P, TKN, COD) that represented the range of influent characteristics based on historical influent data for each WRRF treatment alternative (Figure 1a). The generated samples were subsequently used to train and validate ANNs to predict the treatment performance of each alternative in various combinations of influent characteristics within the defined range (Table 1).

2.2. Development of ANNs as Efficient Surrogates for **Five WRRF Models.** Fully connected feed-forward backpropagation ANNs,³⁰ consisting of multilayer perception (MLP), were trained as surrogate models for the five WRRF treatment alternatives (Figure 1b). The first MLP layer represented the input layer with each node being one input variable while the last layer represented the output layer with each node being one output variable. The hidden layers between input and output layers were used to approximate nonlinear behavior between inputs and outputs. Since the configurations of the five WRRF treatment alternatives were based on an existing WRRF, the input variables for the ANNs only included the four influent characteristics that were historically measured, including total flow (sum of wastewater and rainwater flow), TP, TKN, and COD. The output variables consisted of multiple effluent variables of interest, including COD, TP, TSS, TN, nitrate, sludge production, total aeration requirement (for energy consumption estimation), as well as struvite formation and recovery in the EBPR layouts.

Among the 10 000 simulations, we found that as the complexity of the WRRF model increased, there was a subsequent increase in the number of simulations that failed to reach a steady state solution. There are two possible causes responsible for failure runs. First, certain extreme combinations of undesirable conditions could result in failed simulations, especially in EBPR layouts that are considered more complex than AS and ASCP layouts. For example, as the influent wastewater composition was randomly generated, there could be instances of highly imbalanced COD/TP ratios causing excessively long computation time that did not reach steady state. Second, EBPR layouts require more computational resources to solve simulations, which in combination with hardware limitations, resulted in shutdown of GPS-X before converging to a steady state solution in certain cases. Therefore, those failed simulations did not represent a normal wastewater treatment performance, and it was necessary to remove those runs, otherwise the data would be contaminated and propagate uncertainty to ANNs. We removed failed simulations from the dataset if they met one of the two criteria: (1) low newberyite concentration in anaerobic digestor (<1 mg MgHPO₄·3H₂O L⁻¹); newberyite in anaerobic digestor is a byproduct that was predicted to form within a system abundant with polyphosphate accumulating organisms

(PAOs); or (2) extremely low nitrate effluent (<0.001 mg $\rm NO_3-N~L^{-1}$) as a result of highly imbalanced and unfavorable influent composition that typically did not reach steady state. After removing the failed runs, the dataset for each WRRF model was randomly divided into three groups (60% as training, 20% as validation, 20% as testing) for ANN training and validation. Lastly, a 5-fold cross-validation method was further applied to validate the ANNs trained in this work.

The input combinations of influent characteristics and GPS-X simulation outputs were normalized between 0 and 1 to avoid undesired impacts due to unit differences between inputs and outputs. Hyperparameters (e.g., number of hidden layers, neurons, learning rates, algorithms for optimizing weights) of ANNs were chosen based on trial and error, including the activation functions, learning rates, the number of neurons in hidden layers, the number of hidden layers, etc. By trial and error, we considered two of the most widely used activation functions to convert linear combinations of weighted neurons into nonlinear relationships: rectified linear (ReLu) unit ($\sigma = \max(0, x)$), and Sigmoid ($\sigma = \frac{e^x}{e^x+1}$) where x is the normalized input to neurons. The learning rate was selected as 0.01, the number of neurons as n = 20, and the number of hidden layers as two. The generic form of ANN structure can be described using eqs 1–3:

$$f_{l,n} = \sigma_l(\mathbf{W}_{l,n}^{\mathrm{T}}. \mathbf{a}_{l-1} + \mathbf{b}_{l,n})$$
(1)

$$f_l = \{f_{l,1}, \dots, f_{l,n-1}, f_{l,n}\}$$
(2)

$$f_{\text{ANN}}(\mathbf{x}) = f_{\text{output}}(f_{\text{h2}}(f_{\text{h1}}(x)))$$
(3)

where $f_{l,n}$ is the output from neuron n in layer l, where l \in {hidden layer 1(h1), hidden layer 2(h2), output}, σ_l is the activation function used in layer l, a_{l-1} is the vector of inputs from previous layer l-1, $W_{l,n}$ is the vector of weights for the neuron n in layer l, $\mathbf{b}_{l,n}$ represents the vector of bias for neuron *n* in layer *l*, and f_l is the *l*th layer of neurons. f_{ANN} is hierarchically composed of each layer, starting from the input layer, hidden layers, and the output layer. The weights and bias in each neuron and each layer were optimized by Adam solver (a widely used stochastic optimization algorithm) to minimize the error on training data during the backpropagation process.³¹ The ANN surrogate models were trained using the "Keras" package in Python. The performance of trained ANNs was evaluated using two commonly used metrics for the predictive accuracy of the ANNs: mean square error (MSE) and coefficient of determination (R^2) .

2.3. Long-Term Simulation with Monthly Average in ANN. To evaluate the long-term simulation of nutrient removal in each WRRF treatment scenario, we simulated monthly loading over a period of 10 years (2006-2015). For each month, the total inflow (domestic and industrial wastewater + rainwater), TKN, and TP were randomly sampled 1,000 times with triangular distributions (Figure 1c). Triangular distributions, rather than fitted distributions for each month were applied due to limitations in monthly data (8-15 data points per month). To reflect monthly influent variability, we chose triangular distributions with minimum, maximum, and mode values determined, using monthly historical data over 10 years (2006-2015) for inflow, TKN, and TP. As historical COD data at a monthly scale was not available, the distribution of COD was assumed to be the same for all months; that is, 1000 samples of influent COD were

sampled each month with the same triangular distribution. The minimum, mode, max values of flow, TP, TKN, COD for each year of the long-term simulations are provided in Table S3. We checked the correlation between influent TKN and TP using historical data and found a weak correlation (Pearson's correlation: r = 0.239 and coefficient of determination: $R^2 = 0.0571$). Therefore, we did not consider their correlation during the Monte Carlo sampling. The correlation was weak because the plant receives most of its influent P from an industrial source (nearly 90%), and most of its N from domestic sources.

Calibrating a dynamic long-term period (e.g., 10 years) simulation in GPS-X could be challenging for three reasons. First, the lack of detailed knowledge of real-time influent wastewater characteristics and how rainfall translates to plant influent characteristics could introduce uncertainty. Without this information, it was not possible to calibrate and validate a dynamic model. Second, process modifications at the real WRRF made in 2011 and other key external variables (e.g., temperature) that have significant impacts on the treatment performance, were difficult to incorporate for long-term simulations. Third, to generate sufficient data for the ANN training within a reasonable amount of time, both the process layout and operational considerations were simplified. To simulate the long-term treatment performance, we limited simulation failures in higher complexity process layouts by using a single aeration basin and steady-state operation. We further assumed that each month was a steady-state and used monthly average values to represent the states. Details of each model's performance with simplified treatment layouts are provided in section 3.3.

2.4. Techno-economic Analysis of WRRF Models. Full plant layouts were built in CapdetWorks (v4.0; Hydromantis Environmental Software Solutions, Inc.) to calculate the fixed costs of capital construction and equipment, labor, and supply materials for the five WRRF models (Figure 1d). CapdetWorks provides comprehensive vendor data for cost estimation of construction projects related to wastewater treatment plants. Direct costs include site preparation, mobilization, and yard piping, while indirect costs include design fee, inspection, contingency, etc. The labor and maintenance costs were also estimated with CapdetWorks. The capital, labor, and maintenance costs for the five WRRF models are provided in Supporting Information (SI), Table S4. As a single struvite recovery reactor unit process was not available in Capdet-Works, a continuous stirred tank reactor (CSTR) with similar dimensions was added instead. It is important to note that the capital cost of a fluidized bed struvite reactor may be greater than a CapdetWorks CSTR reactor (because of the special equipment and the reactor body material), but this was done as an approximation to account for the total cost differences between the EBPR and EBPR-S processes. Variable operational costs that change with influent conditions (e.g., flow rate, phosphorus, COD) were calculated with engineering design equations derived from the literature and GPS-X manual.³² Specifically, the variable operational costs included (1) aeration energy, (2) pumping energy, (3) heating energy, (4) mechanical mixing energy, (5) miscellaneous energy, (6) chemical dosage, and (7) sludge disposal costs. Among those operational costs, the pumping energy, heating, and sludge disposal costs were based on the outputs (e.g., aeration requirement, sludge production) predicted by ANNs (Figure 3d). It is recognized that TEA results could be highly

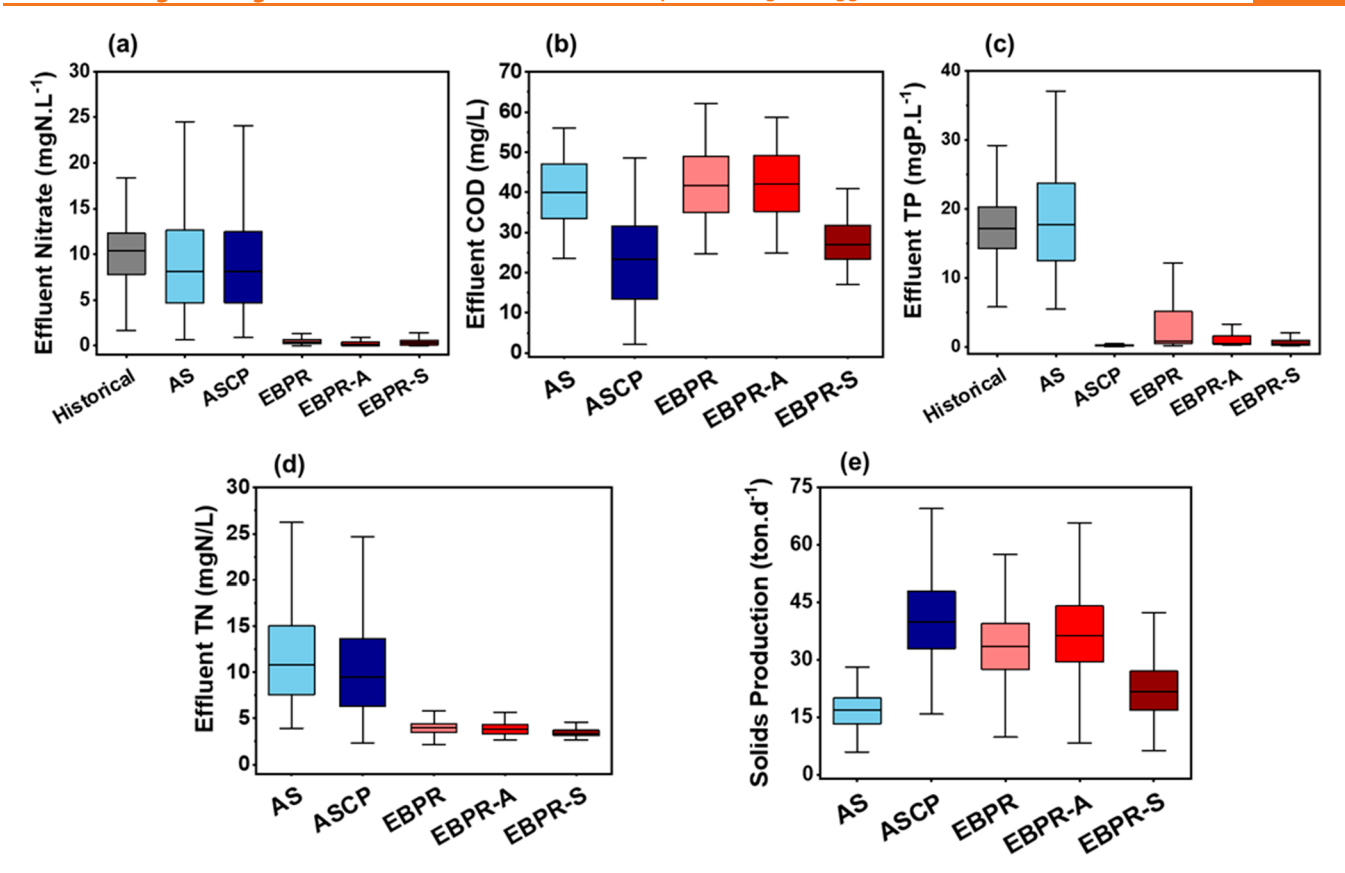


Figure 2. GPS-X Simulation results of five WRRFs treatment alternatives under 10000 Monte Carlo samples: nitrate effluent (a); COD effluent (b); TP effluent (c); TN effluent (d); biosolids production (e).

uncertain, given the fact that unit costs vary across spatial and temporal scales, such as costs associated with chemical additives. For a transparent comparative analysis, we have provided detailed parameters and major unit costs applied in this study in SI, Tables S3–S9. The discount rate for capital costs was set at 3% based on the US EPA's Water Infrastructure Finance Innovation Act (WIFIA) program, while the discount rate for annual operating costs was assumed to be 7%. From the operating and capital costs, the equivalent annual cost (EAC, \$/yr) of the five developed WRRF models was calculated to allow for comparison of the cost effectiveness of annual nutrient removal across different WRRF alternatives.

To compare the normalized life cycle cost of nutrient removal for different treatment alternatives, we calculated the normalized cost ($C_{\text{Nutrient},i}$, \$/ Δ kg nutrient removed) of nutrient removal (both N and P) relative to the baseline AS process:

$$C_{\text{Nutrient},i} = \frac{\text{cost}_{i} - \text{cost}_{\text{AS(baseline)}}}{\text{Nutrient}_{\text{eff,AS(baseline)}} - \text{Nutrient}_{\text{eff,i}}}$$
(4)

where Cost_i (\$/year) represents the annualized cost for treatment alternative $i \in \{\operatorname{ASCP}, \operatorname{EBPR}, \operatorname{EBPR-A}, \operatorname{EBPR-S}\}$. Nutrient $_{\operatorname{eff},i}$ is the nutrient effluent (N or P, kg/yr) for treatment alternative i. $\operatorname{Cost}_{\operatorname{AS(baseline)}}$ and Nutrient $_{\operatorname{eff},\operatorname{AS(baseline)}}$ represent the treatment cost and nutrient effluent for the baseline (AS), respectively. Note that in all cases, every treatment alternative had higher nutrient removal and higher costs compared to the baseline. Because of this, cases of negative normalized costs or cheaper but less effective treatments did not exist in our data set.

3. RESULTS AND DISCUSSION

3.1. GPS-X Simulation Results. 3.1.1. Comparison of WRRF Models and Historical Data. Simulated effluent nitrate concentrations in AS and ASCP processes were comparable to historical data (Figure 2a). Since a uniform distribution for influent data was used to generate sufficient variability for ANN training, the number of days with rain events was higher in influent data than in historical data, leading to simulated nitrate results with greater variability. Although simulated AS effluent nitrate and historical data were within the same range, our simulations had slightly lower median concentrations. Since partial denitrification was employed in the WRRF, changes in controlled DO values over time could impact the denitrification rate.³⁴ As we only had access to data pertaining to very recent controlled DO values in the plant, the lower median simulated effluent nitrate concentrations could be explained by historical differences in DO values used in the aeration basins of the plant. Analysis on historical data further revealed that effluent nitrate loadings were always higher than influent ammonia, which could be caused by extra nitrogen loads from a solids handling lagoon located in the vicinity of the WRRF. This indicates that nitrification may not have been the sole contributor to effluent nitrate in the historical data, as it could also be affected by external nitrogen loads from the lagoon. Simulated effluent TP concentration in the AS process was in good agreement with the historical data as sludge/ hydraulic retention time, aeration basin volume, and sludge settling capacity used in the models were consistent with the WRRF. In terms of COD removal, all treatment alternatives had acceptable performance to meet standard discharge limits,

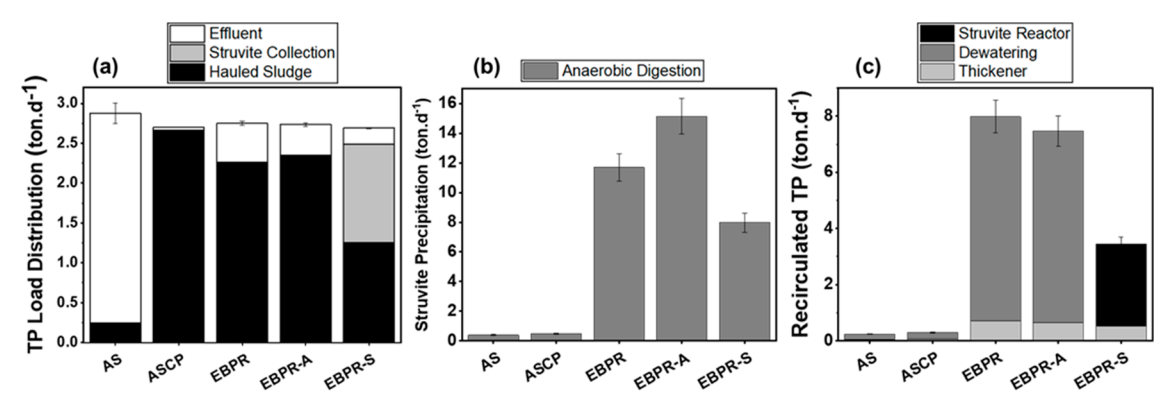


Figure 3. Phosphorus mass balance, precipitation, and recirculation in WRRF GPS-X simulations. TP distribution in plant output streams (a); uncontrolled struvite precipitation in the AD unit (b); and recirculated phosphorus from solids handling operations (c). Error bars represent the standard error of the average values.

with ASCP and EBPR-S having the lowest effluent COD concentrations (Figure 2b).

Effective chemical and enhanced biological TP removal was observed in all treatment alternatives. ASCP had the highest removal (lowest effluent TP concentration), followed by enhanced biological TP removal processes. EBPR performance was improved with the addition of acetate or with side-stream phosphorus recovery. In the ASCP process simulations, TP concentration decreased significantly from an average influent concentration of 25, to 0.25 ± 0.10 mgP/L in the effluent (Figure 2c). This was attributed to the formation of ferric hydroxide and ferric phosphate.³⁵ Simulated biological phosphorus removal processes also showed significant removal efficiencies. EBPR-A had higher TP removal efficiency compared with basic EBPR, showing the positive impact of maintaining a C/P ratio between 26 and 30 to avoid PAO carbon limitations.³⁶ EBPR-S had the highest removal efficiency and narrowest effluent TP range as it dramatically reduced the amount of P returning from solids digestion and thickening operations to mainline treatment, alleviating carbon limitations and reducing sludge production (Figure 2c).3

Nitrification and partial denitrification in the AS process led to a reduction in effluent TN concentration. This reduction was slightly improved in the ASCP process, due to increased sludge settleability from chemical addition. Significant biological nitrogen removal was observed in EBPR, EBPR-A, and EBPR-S processes. This is indicative of the reliable performance of anoxic stages for strong denitrification and nitrogen gas stripping, followed by nitrification in aerobic stages leading to the removal of ammonia from the stream (Figure 2d). While iron precipitation resulted in the lowest effluent P concentrations, it significantly contributed to sludge production (Figure 2e). Chemical sludge production is reported to increase linearly with coagulant dosage,³⁷ while extra sludge production in an EBPR process is expected to be between 30 to 60% of that obtained in a chemical process.³⁸

3.1.2. Phosphorus Mass Balance and Recirculation. All four P removal treatment scenarios led to reductions in effluent discharge, but design and operating decisions impacted nutrient recovery and intraplant P recirculation. In the AS process, the majority of influent TP leaves the plant through the effluent, resulting in low P content in hauled sludge, minimal uncontrolled struvite formation during sludge digestion, and little recirculated P from solids handling. In the ASCP process, however, most of the influent TP leaves the plant through hauled sludge, because of the strong chemical

phosphorus removal efficacy, with minimal TP load in the effluent. In this scenario, the P is fixed to iron and there is little remobilization during digestion, resulting in low struvite formation and recirculation. Recent studies have indicated that iron phosphate mineral vivianite forms during the digestion of iron amended sludge.^{39–41} Potential impacts of vivianite scaling on the return conduit were not accounted for in cost estimates.

While all EBPR processes showed significant reductions in TP load leaving the plant through effluent, EBPR-S proved to have the highest TP removal performance, while also channeling 42-58% of influent P to the struvite crystallization reactor (Figure 3a). While the addition of acetate during mainline treatment helped to reduce TP load in the effluent, the re-release of P during solids handling elevated uncontrolled struvite precipitation in the anaerobic digestion (AD) unit when acetate was used (Figure 3b). This also led to higher energy consumption associated with EPBR aeration to reach defined DO set points (EBPR: 4.66-5.69 GWh/yr, EBPR-A: 4.77-9.21 GWh/yr, EBPR-S: 3.87-4.82 GWh/yr). Furthermore, the inclusion of a post digestion struvite crystallizer reduced P cycling from solids handling operations (Figure 3c) This reduction was highly impactful as the P returning from solids handling was much greater than the plant influent load. Cascading impacts could be observed in the P content of hauled sludge and uncontrolled struvite precipitation in the digester.

3.2. ANNs Simulation Performance for the Five WRRF Models. The ANN and GPS-X simulation outputs including nutrient effluent concentrations (nitrate, TN, TP), biosolids production, airflow demand for aerobic reactors, and recovered struvite (EBPR-S only) exhibited a strong correlation, with overall R-squared higher than 0.985 and MSE lower than 0.0005 for all five plant-wide models (Figure 4). As the model complexity increased from activated-sludge-based layouts to EBPR-based layouts, R-squared slightly decreased for EBPR-S (from 0.998 for AS to 0.974). Although the impact of model complexity seemed to be negligible on ANNs performance, it had a considerable impact on the number of failed simulations. For example, no outliers were detected for the AS and ASCP layouts, while 2878 and 1786 failed simulations (out of 10 000) were detected in EBPR-A and EBPR-S layouts, respectively. The removal of outliers from failed GPS-X steady-state simulations was the key to the success of developing surrogate WRRF models with ANNs. Before training ANNs without removing outliers, the R-squared

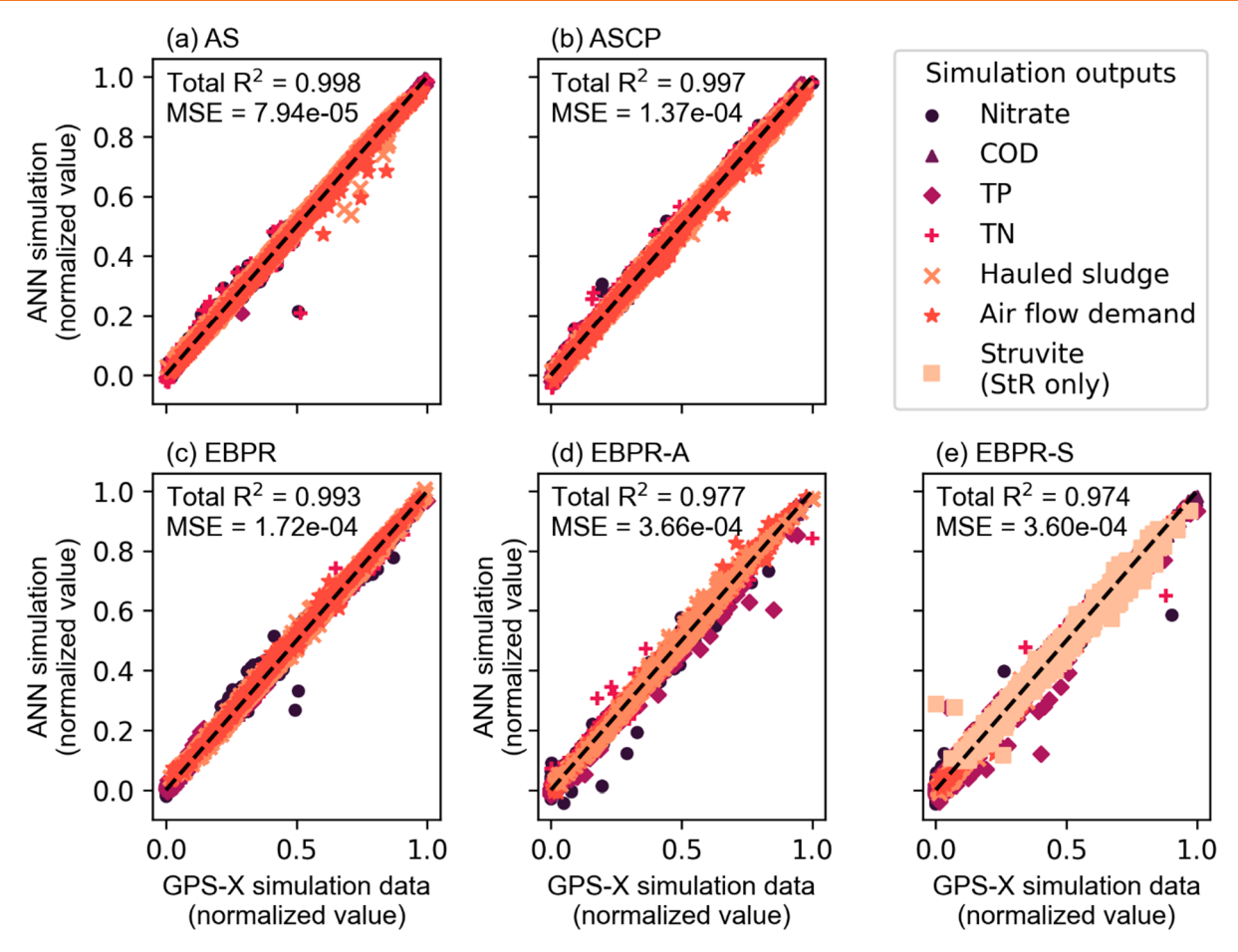


Figure 4. Simulation outputs from GPS-X and ANNs in evaluating test data (20% of the data set). Subplots include (a) activated sludge (AS); (b) activated sludge with chemical precipitation (ASCP); (c) modified Bardenpho enhanced biological phosphorus removal (EBPR); (d) EBPR with acetate (EBPR-A); (e) EBPR with struvite recovery (EBPR-S). Total R^2 and MSE are calculated based on 5-fold cross validation.

used as an indicator for ANNs performance was 0.90 (as compared to 0.99 after data filtering).

In addition to ANNs, there have been other reported suitable surrogate models such as random forest, Kriging, radial basis functions, and different variants of ANNs (e.g., long short-term memory). 24,25 In our study, we did not explicitly compare the performances among different surrogate methods, but rather focused on developing surrogate models with satisfactory performance to apply them for efficient long-term simulations. It is also noted that additional uncertainty is introduced when applying surrogate models. There are multiple ways to quantify the uncertainty associated with the ANNs, such as Bayesian or bootstrap approaches. 42,43 We did not quantify the uncertainty of ANN models because (1) the uncertainty introduced by ANN models was considered to be small as R-squared values were very high; (2) the uncertainty analysis could increase the computation time for ANN models. For example, the bootstrap-based approach would create an ensemble of ANNs for the same WRRF treatment alternative, of which the computation time will depend on the number of ANN instances created within an ensemble.44

3.3. Long-Term Simulation of Wastewater Treatment under Wet and Drought Weather. Following ANN training and validation, the plant-wide surrogate models were used to simulate long-term nutrient removal performance (Figure 5) using 10 years of historical influent data. The AS treatment alternative predicted by ANN showed a similar

concentration range to the historical nitrate and TP loading using the typical ranges of influent characteristics (Figure 5a). Our approach to long-term simulation, with the assumption that each month is a steady-state and can be represented by the monthly average effluents, has two advantages. First, the 1000 ANN simulations in ANNs based on average historical monthly influent characteristics could be executed within seconds, compared with a high-fidelity computer program using a Matlab-controlled script, which took hours or days (dependent on model complexity) in GPS-X. Second, WRRF treatment performance could be easily simulated under alternate future climate scenarios as long as the relationship between precipitation and inflow was known. The relationship between precipitation in different climate scenarios can be predicted using historical precipitation data and inflow data. While there are clear strengths, our approach has its limitations. First, such simplification could lead to discrepancy in effluent simulation. Second, our WRRF models were based on steady-state simulations and could not be used to predict the impact of extreme short-term events.

When compared historical nitrate loading with the AS using monthly influent characteristics distribution over 10 years, the nitrate loading of AS predicted by ANN had a 22700 kg/month underestimation (38%) (Figure 5b). The historical data included wet (2008–2010) and drought (2011 June to 2013) periods, allowing for an understanding of how different treatment alternatives could respond to climate variability.

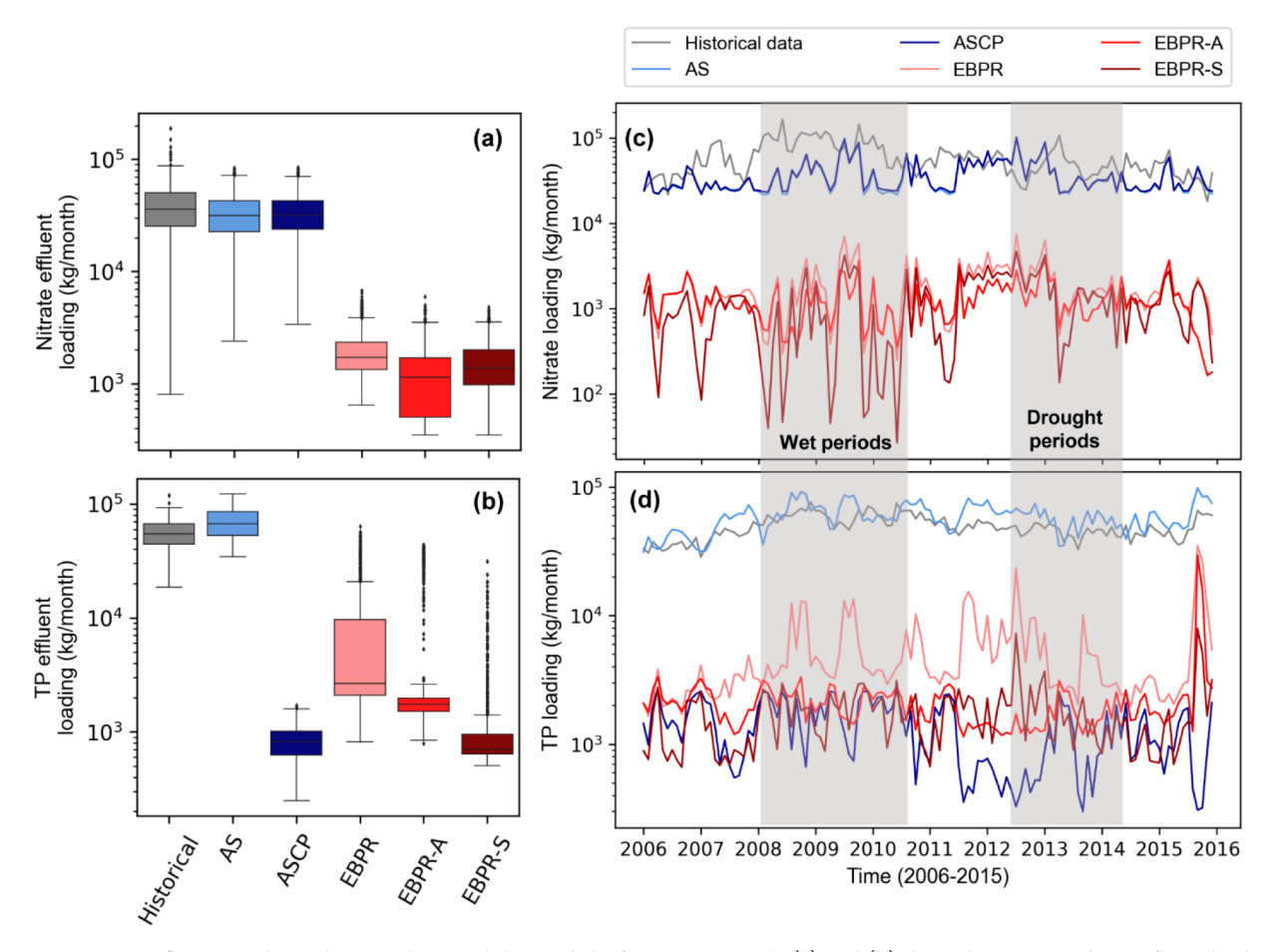


Figure 5. Nutrient effluent simulation between historical data and the five ANNs. Panels (a) and (b) show the nitrate and TP effluent loading for historical data and the five WRRF treatment alternatives using typical ranges of influent characteristics presented in Table 1, respectively. Boxes represent 25 (Q1), 50 (Q2, median), and 75% (Q3) quartiles. Interquartile range (IQR) = Q3–Q1; whiskers represent values of Q1 – 1.5IQR (lower bound) and Q3 + 1.5IQR (upper bound), and dots represent statistical outliers. Panels (c) and (d) show historical data and long-term dynamic simulation of nitrate and TP using long-term monthly influent characteristics presented in Figure 2c, respectively.

The discrepancy observed between ANN nitrate loading simulations and historical data was more significant during wet periods when the plant received flushes of stormwater from the combined sewer system (Figure 5c). As discussed in section 3.1, based on the analysis performed on historical data, it was suspected that nitrogen loading discharge from a lagoon near the wastewater treatment plant could also contribute to the effluent nitrate loading. However, the effluent nitrate loadings predicted by the AS simulation model and ANN were only a result of nitrification in the aeration basins, which could be a source for the discrepancy between historical and simulated data. Moreover, effluent nitrate loading in historical data could be impacted by seasonal temperature variations and inconsistent DO control strategies, especially during severe rain events when increased aeration was required to maintain optimum aerating conditions. Nitrite peaks have been reported to be caused by a drop in oxygen concentration along with spikes of TKN concentration in the influent, while increasing aeration was only proven to be beneficial to effluent quality and N₂O emission up to a certain threshold.⁴⁵ Therefore, possible inconsistency in aeration control during wet periods could lead to increased effluent nitrate concentrations from the plant. Also, since the temperature was kept constant in our simulations, the ANNs could not have captured the impact of temperature on denitrifying bacteria community and their subsequent effect on nitrate reduction. A variance-based

sensitivity analysis applied to an integrated activated sludge model (ASM2d) revealed that maximum growth rate, growth yield, and decay rate for heterotrophic bacteria introduced the highest variance to nitrate concentration.⁴⁶ While the growth rate was increased at high temperatures, 47 cell decay rate was reported to be slower at low temperatures. 48 Therefore, it is likely that the ANNs did not fully capture the seasonal variations in activated sludge activity at the plant. Furthermore, influent readily biodegradable and inert particular COD also have a significant impact on effluent nitrate concentrations, as a lower degradable COD fraction could mean reduced denitrification and higher effluent nitrate concentrations. 49 Therefore, uncertainty in the influent COD fractions of the historical data and ANN simulations could lead to additional discrepancies. Finally, the actual plant has gone through operational modifications since 2011; as our simulations were based on the most recent characteristics of the plant, this could explain why the discrepancy between the historical data and simulated effluent nitrate loading rates was most significant before 2011 (Figure 5c).

Although our approach showed that estimates of nitrate loading over a long-term period can result in significant discrepancy, point source nitrate loading typically contributes a small portion of total nitrate loading for agricultural watersheds, compared to the nonpoint source nitrate from landscape loss. For example, the WRRF in our work only contributes

Table 2. Breakdown of Equivalent Annualized Costs for the Five WRRF Treatment Alternatives

WRRF alternative	fixed cost ^a	energy cost ^b	chemical cost ^b	sludge handling cost ^b	revenue of struvite ^b	total cost ^b
AS	16.73	0.91	0.15	0.04		17.82
		[0.77,1.05]	[0.14,0.17]	[0.03, 0.05]		[17.68, 17.99]
ASCP	17.10	0.91	0.85	0.10		18.94
		[0.78, 1.05]	[0.58, 1.19]	[0.07, 0.12]		[18.81, 19.34]
EBPR	18.53	0.70	0.16	0.08		19.47
		[0.66, 0.78]	[0.14, 0.17]	[0.07, 0.11]		[19.41, 19.57]
EBPR-A	18.53	0.77	3.82	0.09		23.21
		[0.67, 1.11]	[0.58, 8.32]	[0.07, 0.12]		[19.43, 28.02]
EBPR-S	18.72	0.65	1.79	0.06	0.59	20.62
		[0.61, 0.73]	[1.46, 2.27]	[0.04, 0.08]	[0.27, 1.18]	[20.27, 28.36]

^aNote: Fixed cost includes capital cost, labor cost, maintenance cost, and material cost. ^bAll values are in unit \$Million/year. Values within the bracket represent the range of 95% confidence interval.

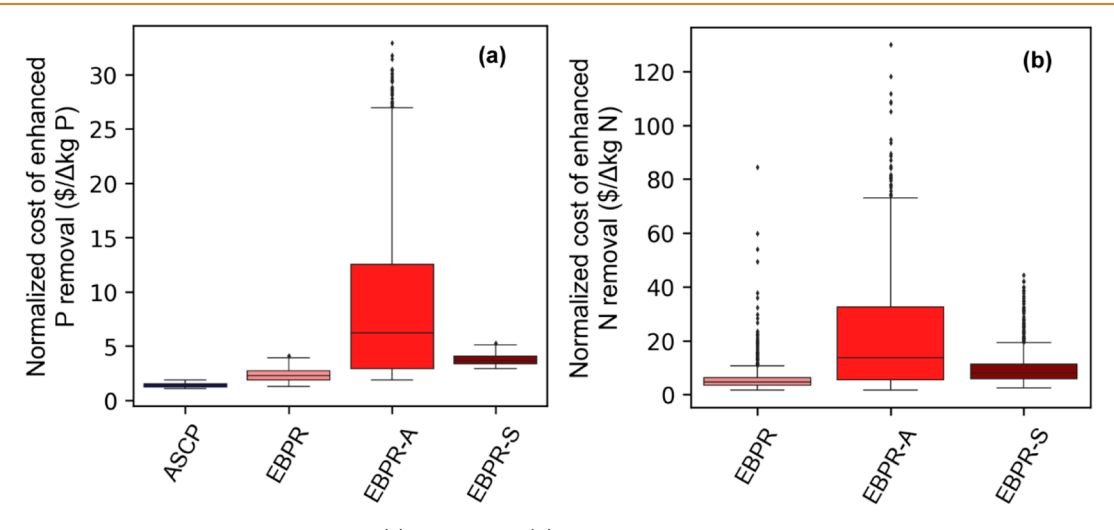


Figure 6. Normalized cost of enhanced phosphorus (a) and nitrate (b) removal related to activated sludge. Calculation of normalized costs are based on eq 4.

7.5% of total nitrate loading in the watershed. A 38% underestimation of point source nitrate will lead to an overall 2.9% underestimation for the watershed, which is acceptable for future watershed optimization efforts.

Compared with the nitrate simulation, TP loading simulations compared favorably to historical data (Figure 5d). The TP loading from AS followed the trend of historical TP loading and the discrepancy was much smaller (18% overestimate on average), as compared to the case of nitrate loading. ASCP had the best performance in removing TP from effluent. Simulation results indicated the notable variability of EBPR performance in reducing effluent TP loading rates. While EBPR-S exhibited a higher degree of performance stability due to reduced P recirculation, EBPR and EBPR-A had a fluctuating performance, especially during wet/drought periods. These wet/drought periods subjected the simulated models to intense variations in influent flow, leading to fluctuations in HRT values in anaerobic, anoxic, and aerobic basins. Shifts in the HRT value above or below an optimal range (anaerobic 0.5-1.5, first anoxic 1-3, first aerobic 4-12, second anoxic 2-4, and second aerobic 0.5-1 h²⁸) is reported to adversely affect EBPR performance. 50,51 This would be a major problem for the simulated hypothetical EBPR plants in which the recirculated TP load was so much greater than influent load, as increased rainwater flow would effectively wash out the recirculated P.

3.4. Normalized Lifecycle Cost Comparison of Nutrient Removal Alternatives. Since economic considerations often dictate decision-making when adopting modified or new technologies in WRRFs,⁵² a techno-economic analysis was conducted for each WRRF treatment alternative. The equivalent annual costs differed for each scenario with AS being the lowest and EBPR-S the highest (Table 2). As expected, the greatest contribution to lifecycle cost came from fixed costs (capital, labor, maintenance, and material cost). The chemical cost could vary considerably with treatment alternatives as shown in Table 2. The chemical cost in the baseline (AS) included basic chemical needs (e.g., polymer for sludge thickening, sodium hypochlorite for disinfection) and cost 0.15 \$MM/yr. For ASCP, the amount of iron addition was calculated based on a 1:1 molar ratio of each mole of influent P to one mole of iron (Fe), yielding an increase in the chemical cost to 0.85 \$MM/yr on average. EBPR-A had the highest chemical costs (\$3.82 MM/yr) due to acetate addition. For EBPR-S, the revenue of recovered struvite was estimated at 0.59 \$MM/yr (assuming the recovered struvite is worth \$0.5/ kg). The energy cost, which included aeration, digestion heating, pumping, and miscellaneous uses (mechanical operations, rakes, etc), was lower in the three EBPR layouts than the AS and ASCP, mainly due to decreased airflow demand attributed to denitrification. It is also noted that sludge handling costs in ASCP, EBPR, and EBPR-A were more than twice of sludge handling cost in AS, although sludge

handling costs for all treatment alternatives were relatively negligible. However, this cost was based on the amount of sludge production and did not take the impacts of nutrient and heavy metal contents into account, and may underestimate the cost of sludge disposal.

To compare the cost-effectiveness of nutrient removal to baseline AS, we evaluated the incremental cost required for removing additional nutrients (calculation details provided in section 2.4). It was found that ASCP was the most costeffective treatment alternative for removing P, due to its low additional fixed cost and most significant P removal (Figures 2c and 6a). However, it should be noted that the ASCP layout does not provide the nitrogen removal benefits of EBPR (Figure 6b). It is important to acknowledge the uncertainty of cost inputs to these estimates as chemical costs can vary highly depending on the region and time of purchase; moreover, the capital cost estimation for the struvite crystalization reactor was probably an underestimation, because this specific unit process was not defined in CapdetWorks. To reduce chemical cost uncertainty, we searched bid tabulations online to estimate the bulk price of ferric chloride, acetate, magnesium chloride, and sodium hydroxide (SI, Table S9). Owing to the uncertainty of the cost of chemicals, the estimated operational costs could be different, and depend on the location and time of alternative scenarios. Given the lack of an struvite fluidized bed reactor unit process in CapdetWorks, we designed a concrete CSTR and settling basin for sidestream P recovery, which could underestimate the fabrication cost of the high aspect ratio (height/width) reactors often employed in the field.

The normalized costs of N and P removal were lowest for EBPR when chemical addition and struvite precipitation were excluded. However, as noted earlier, EBPR without chemical amendments is highly sensitive to influent conditions, which could lead to discharge permit violations (e.g., 1 mg/L TP). The normalized nutrient removal costs of EBPR-A exhibited the largest variability in removing P as its chemical cost is related to the ratio of COD and TP in the influent, which can have a high variability. The normalized cost of P removal with EBPR-S was slightly higher than ASCP and EBPR, but simulations indicated that it would provide the most stable removal performance while generating a renewable fertilizer product. Therefore, when considering both nitrate and TP removal as well as the stability of cost-effectiveness, EBPR-S appeared to be the best alternative, particularly if coupled with side-stream sludge fermentation for in-situ volatile fatty acid production to reduce mainline carbon limitations. It should also be noted that due to the limitations mentioned earlier, the capital cost estimation for the EBPR-S process could be an underestimation and subject to uncertainty. This uncertainty in capital cost estimation should be taken into account before making final conclusions about the cost-effectiveness of the EBPR-S process.

There have been efforts in the literature to model eutrophication in a unified metric considering spatial and temporal factors. ^{53,54} Comparing the cost-effectiveness of nutrient removal on such a unified metric would be beneficial for a more holistic comparison, and is suggested for future studies.

4. OUTLOOK

In this study, we applied a novel approach to compare the long-term nutrient removal performance and cost-effectiveness of five WRRF treatment alternatives. We first developed five high-fidelity WRRF models in GPS-X simulation software, and then applied ANNs to surrogate the five WRRF models with satisfactory performance. The developed ANN models showed the capability of predicting the treatment performance of all WRRFs under stochastic influent characteristics with a good degree of accuracy. Removing failed simulations was a key step in ensuring the success of the ANNs' development. Our study highlighted the benefit of side-stream P recovery as demonstrated both in process-based and ANN models. Specifically, EBPR-S showed the highest treatment stability, while EBPR without chemical addition was very sensitive to influent flow rate and composition.

Applying the ANN models for long-term simulation can significantly reduce the computational burden with acceptable accuracy, which can facilitate the coupling of complex process models. For example, the ANN models that represent point-source nutrient removal and recovery have been coupled with other hydrological models that simulate nonpoint source contributors, while implementing economic models to evaluate nonmarket valuations for water quality improvement in an integrated watershed optimization framework. This methodolgy could allow for a holistic watershed nutrient management practice. ¹¹

ASSOCIATED CONTENT

Supporting Information

The Supporting Information is available free of charge at https://pubs.acs.org/doi/10.1021/acsestengg.1c00179.

Descriptions of plant layouts and design parameters, equations, and parameters used in techno-economic analysis for cost estimates (PDF)

AUTHOR INFORMATION

Corresponding Author

Roland D. Cusick — Department of Civil and Environmental Engineering, University of Illinois at Urbana—Champaign, Urbana, Illinois 61801, United States; ocid.org/0000-0002-4037-2939; Phone: +1(217) 244-6727;

Email: rcusick@illinois.edu

Authors

Shaobin Li — Department of Civil and Environmental Engineering, University of Illinois at Urbana—Champaign, Urbana, Illinois 61801, United States; occid.org/0000-0001-8930-426X

Seyed Aryan Emaminejad – Department of Civil and Environmental Engineering, University of Illinois at Urbana–Champaign, Urbana, Illinois 61801, United States

Samuel Aguiar — Department of Civil and Environmental Engineering, University of Illinois at Urbana—Champaign, Urbana, Illinois 61801, United States

Aliza Furneaux — WateReuse Association, Alexandria, Virginia 22314, United States

Ximing Cai — Department of Civil and Environmental Engineering, University of Illinois at Urbana—Champaign, Urbana, Illinois 61801, United States

Complete contact information is available at: https://pubs.acs.org/10.1021/acsestengg.1c00179

Author Contributions

[#]S.L. and S.A.E. are cosenior authors.

Notes

The authors declare no competing financial interest.

ACKNOWLEDGMENTS

This work was supported by the US National Science Foundation, Innovations at the Nexus of Food, Energy and Water Systems (INFEWS/T1) award No.1739788. We thank the existing utility partner in Illinois, USA, for providing valuable information for modeling WRRF alternatives, and Tomas Johnson from Jacobs Engineering Group Inc. for providing valuable suggestions on cost estimates.

REFERENCES

- (1) Mitchell, J. K.; McIsaac, G. F.; Walker, S. E.; Hirschi, M. C. Nitrate in River and Subsurface Drainage Flows from an East Central Illinois Watershed. *Trans. ASAE* **2000**, *43* (2), 337–342.
- (2) Ulloa, M. J.; Álvarez-Torres, P.; Horak-Romo, K. P.; Ortega-Izaguirre, R. Harmful Algal Blooms and Eutrophication along the Mexican Coast of the Gulf of Mexico Large Marine Ecosystem. *Environ. Dev.* **2017**, 22, 120–128.
- (3) EPA Science Advisory Board. Hypoxia in the Northern Gulf of Mexico: An Update by the EPA Science Advisory Board; EPA: Washington, DC, 2007.
- (4) NOAA. Happening Now: Dead Zone in the Gulf 2020 https://oceantoday.noaa.gov/happenowdeadzone/ (accessed July 25, 2021).
- (5) Illinois Environmental Protection Agency; Illinois Department of Agriculture. *Illinois Nutrient Loss Reduction Strategy*; University of Illinois Extension: 2015.
- (6) Rao, N. S.; Easton, Z. M.; Schneiderman, E. M.; Zion, M. S.; Lee, D. R.; Steenhuis, T. S. Modeling Watershed-Scale Effectiveness of Agricultural Best Management Practices to Reduce Phosphorus Loading. *J. Environ. Manage.* **2009**, *90* (3), 1385–1395.
- (7) Song, J.; Gramig, B. M.; Cibin, R.; Chaubey, I. Integrated Economic and Environmental Assessment of Cellulosic Biofuel Production in an Agricultural Watershed. *BioEnergy Res.* **2017**, *10* (2), 509–524.
- (8) Reports on Point Source Progress in Hypoxia Task Force States; US EPA: Washington, DC, 2019.
- (9) Zhang, Ž.; Huang, J.; Xiao, C.; Huang, J. C. A Simulation-Based Method to Develop Strategies for Nitrogen Pollution Control in a Creek Watershed with Sparse Data. *Environ. Sci. Pollut. Res.* **2020**, 27 (31), 38849–38860.
- (10) Cai, X.; Wallington, K.; Shafiee-Jood, M.; Marston, L. Understanding and Managing the Food-Energy-Water Nexus Opportunities for Water Resources Research. *Adv. Water Resour.* **2018**, *111*, 259–273.
- (11) Li, S.; Cai, X.; Emaminejad, S. A.; Juneja, A.; Niroula, S.; Oh, S.; Wallington, K.; Cusick, R. D.; Gramig, B. M.; John, S.; McIsaac, G. F.; Singh, V.; et al. Developing an Integrated Technology-Environment-Economics Model to Simulate Food-Energy-Water Systems in Corn Belt Watersheds. *Environ. Model. Softw.* **2021**, *143*, 105083.
- (12) Mu'azu, N. D.; Alagha, O.; Anil, I. Systematic Modeling of Municipal Wastewater Activated Sludge Process and Treatment Plant Capacity Analysis Using GPS-X. Sustainability 2020, 12 (19), 1–26.
- (13) Bisinella De Faria, A. B.; Sp Erandio, M.; Ahmadi, A.; Tiruta-Barna, L. Evaluation of New Alternatives in Wastewater Treatment Plants Based on Dynamic Modelling and Life Cycle Assessment (DM-LCA). Water Res. 2015, 84, 99–111.
- (14) Makinia, J.; Rosenwinkel, K.-H.; Spering, V. Comparison of Two Model Concepts for Simulation of Nitrogen Removal at a Full-Scale Biological Nutrient Removal Pilot Plant. *J. Environ. Eng.* **2006**, 132 (4), 476–487.
- (15) Sabri, D.; Yassine, D.; Yahia, H.; Dounia, M. Dynamic Simulation for Wastewater Treatment Plants Management: Case of Souk-Ahras Region, North-Eastern Algeria. *J. Water L. Dev.* **2017**, 34 (1), 221–231.

- (16) Troutman, S. C.; Love, N. G.; Kerkez, B. Balancing Water Quality and Flows in Combined Sewer Systems Using Real-Time Control. *Environ. Sci. Water Res. Technol.* **2020**, *6* (5), 1357–1369.
- (17) Leperi, K. T.; Yancy-Caballero, D.; Snurr, R. Q.; You, F. 110th Anniversary: Surrogate Models Based on Artificial Neural Networks to Simulate and Optimize Pressure Swing Adsorption Cycles for CO2 Capture. *Ind. Eng. Chem. Res.* **2019**, *58*, 18241.
- (18) Lu, D.; Ricciuto, D. Efficient Surrogate Modeling Methods for Large-Scale Earth System Models Based on Machine-Learning Techniques. *Geosci. Model Dev.* **2019**, *12*, 1791–1807.
- (19) Zhang, X.; Srinivasan, R.; Van Liew, M. Approximating SWAT Model Using Artificial Neural Network and Support Vector Machine. *J. Am. Water Resour. Assoc.* **2009**, *45* (2), 460–474.
- (20) Liao, M.; Kelley, S. S.; Yao, Y. Artificial Neural Network Based Modeling for the Prediction of Yield and Surface Area of Activated Carbon from Biomass. *Biofuels, Bioprod. Biorefin.* **2019**, *13*, 1015.
- (21) Hamed, M. M.; Khalafallah, M. G.; Hassanien, E. A. Prediction of Wastewater Treatment Plant Performance Using Artificial Neural Networks. *Environ. Model. Softw.* **2004**, *19* (10), 919–928.
- (22) Mjalli, F. S.; Al-Asheh, S.; Alfadala, H. E. Use of Artificial Neural Network Black-Box Modeling for the Prediction of Wastewater Treatment Plants Performance. *J. Environ. Manage.* **2007**, 83 (3), 329–338.
- (23) Choi, D. J.; Park, H. A Hybrid Artificial Neural Network as a Software Sensor for Optimal Control of a Wastewater Treatment Process. *Water Res.* **2001**, *35* (16), 3959–3967.
- (24) Al, R.; Behera, C. R.; Zubov, A.; Sin, G. Systematic Framework Development for the Construction of Surrogate Models for Wastewater Treatment Plants. *Comput.-Aided Chem. Eng.* **2018**, *44*, 1909–1914.
- (25) Pisa, I.; Santin, I.; Morell, A.; Vicario, J. L.; Vilanova, R. LSTM-Based Wastewater Treatment Plants Operation Strategies for Effluent Quality Improvement. *IEEE Access* **2019**, *7*, 159773–159786.
- (26) Meirlaen, J.; Huyghebaert, B.; Sforzi, F.; Benedetti, L.; Vanrolleghem, P. Fast, Simultaneous Simulation of the Integrated Urban Wastewater System Using Mechanistic Surrogate Models. *Water Sci. Technol.* **2001**, *43* (7), 301–309.
- (27) Yaqub, M.; Asif, H.; Kim, S.; Lee, W. Modeling of a Full-Scale Sewage Treatment Plant to Predict the Nutrient Removal Efficiency Using a Long Short-Term Memory (LSTM) Neural Network. *J. Water Process Eng.* **2020**, *37*, 37.
- (28) Tchobanoglous, G.; Burton, F. L.; Tsuchihashi, R.; Stensel, H. D. Wastewater Engineering: Treatment and Resource Recovery, 5th, ed.; Metcalf & Eddy Inc, 2013.
- (29) Wang, R.; Eckelman, M. J.; Zimmerman, J. B. Consequential Environmental and Economic Life Cycle Assessment of Green and Gray Stormwater Infrastructures for Combined Sewer Systems. *Environ. Sci. Technol.* **2013**, 47 (19), 11189–11198.
- (30) Svozil, D.; Kvasnička, V.; Pospíchal, J. Introduction to Multi-Layer Feed-Forward Neural Networks. *Chemom. Intell. Lab. Syst.* **1997**, 39, 43–62, DOI: 10.1016/S0169-7439(97)00061-0.
- (31) Kingma, D. P.; Ba, J. L. Adam: A Method for Stochastic Optimization. 3rd Int. Conf. Learn. Represent. ICLR 2015 Conf. Track Proc. 2015, 1–15.
- (32) Harris, R. W.; Cullinane, M. J.; Sun, P. T. Process Design and Cost Estimating Algorithms for the Computer Assisted Procedure for Design and Evaluation of Wastewater Treatment Systems (CAPDET); Environmental Engineering Division, Environmental Laboratory, U.S. Army Engineer Waterways Experiment Station: 1982.
- (33) Hand, S.; Guest, J. S.; Cusick, R. D. Technoeconomic Analysis of Brackish Water Capacitive Deionization: Navigating Tradeoffs between Performance, Lifetime, and Material Costs. *Environ. Sci. Technol.* **2019**, *53* (22), 13353–13363.
- (34) Wang, J.; Yang, H.; Liu, X.; Wang, J.; Chang, J. The Impact of Temperature and Dissolved Oxygen (DO) on the Partial Nitrification of Immobilized Fillers, and Application in Municipal Wastewater. *RSC Adv.* **2020**, *10* (61), 37194–37201.

- (35) Ifelebuegu, A. O.; Ojo, P. Modelling the Effects of Ferric Salt Dosing for Chemical Phosphorus Removal on the Settleability of Activated Sludge. *J. Environ. Chem. Eng.* **2019**, *7* (5), 103256.
- (36) Majed, N.; Gu, A. Z. Impact of Influent Carbon to Phosphorus Ratio on Performance and Phenotypic Dynamics in Enhanced Biological Phosphorus Removal (EBPR) System Insights into Carbon Distribution, Intracellular Polymer Stoichiometry and Pathways Shifts. *bioRxiv.* **2019**, 671081 bioRxiv June 13.
- (37) Guimarães, N. R.; Ferreira Filho, S. S.; Hespanhol, B. P.; Piveli, R. P. Evaluation of Chemical Sludge Production in Wastewater Treatment Processes. *Desalin. Water Treat.* **2016**, *57* (35), 16346–16352.
- (38) Paul, E.; Laval, M. L.; Sperandio, M. Excess Sludge Production and Costs Due to Phosphorus Removal. *Environ. Technol.* **2001**, 22 (11), 1363–1371.
- (39) Prot, T.; Korving, L.; Dugulan, A. I.; Goubitz, K.; Van Loosdrecht, M. C. M. Vivianite Scaling in Wastewater Treatment Plants: Occurrence, Formation Mechanisms and Mitigation Solutions. *Water Res.* **2021**, *197*, 117045.
- (40) Wilfert, P.; Mandalidis, A.; Dugulan, A. I.; Goubitz, K.; Korving, L.; Temmink, H.; Witkamp, G. J.; Van Loosdrecht, M. C. M. Vivianite as an Important Iron Phosphate Precipitate in Sewage Treatment Plants. *Water Res.* **2016**, *104*, 449–460.
- (41) Wilfert, P.; Dugulan, A. I.; Goubitz, K.; Korving, L.; Witkamp, G. J.; Van Loosdrecht, M. C. M. Vivianite as the Main Phosphate Mineral in Digested Sewage Sludge and Its Role for Phosphate Recovery. *Water Res.* **2018**, *144*, 312–321.
- (42) Kendall, A.; Gal, Y. What Uncertainties Do We Need in Bayesian Deep Learning for Computer Vision? *Adv. Neural Inf. Process. Syst.* **2017**, 2017, 5575–5585.
- (43) Tiwari, M. K.; Chatterjee, C. Uncertainty Assessment and Ensemble Flood Forecasting Using Bootstrap Based Artificial Neural Networks (BANNs). *J. Hydrol.* **2010**, 382 (1–4), 20–33.
- (44) Nourani, V.; Paknezhad, N. J.; Tanaka, H. Prediction Interval Estimation Methods for Artificial Neural Network (ANN)-Based Modeling of the Hydro-Climatic Processes, a Review. *Sustainability* **2021**, *13* (4), 1633.
- (45) Boiocchi, R.; Gernaey, K. V.; Sin, G. Understanding N2O Formation Mechanisms through Sensitivity Analyses Using a Plant-Wide Benchmark Simulation Model. *Chem. Eng. J.* **2017**, *317*, 935–951.
- (46) Cosenza, A.; Mannina, G.; Vanrolleghem, P. A.; Neumann, M. B. Variance-Based Sensitivity Analysis for Wastewater Treatment Plant Modelling. *Sci. Total Environ.* **2014**, 470–471, 1068–1077.
- (47) Rusmana, I. Effects of Temperature on Denitrifying Growth and Nitrate Reduction End Products of Comamonas Testosteroni Isolated from Estuarine Sediment. *Microbiol. Indones.* **2007**, *1* (1), 43–47.
- (48) Wu, S.; Bhattacharjee, A. S.; Weissbrodt, D. G.; Morgenroth, E.; Goel, R. Effect of Short Term External Perturbations on Bacterial Ecology and Activities in a Partial Nitritation and Anammox Reactor. *Bioresour. Technol.* **2016**, 219, 527–535.
- (49) Sin, G.; Gernaey, K. V.; Neumann, M. B.; van Loosdrecht, M. C. M.; Gujer, W. Global Sensitivity Analysis in Wastewater Treatment Plant Model Applications: Prioritizing Sources of Uncertainty. *Water Res.* **2011**, *45* (2), 639–651.
- (50) Brown, P.; Ong, S. K.; Lee, Y. W. Influence of Anoxic and Anaerobic Hydraulic Retention Time on Biological Nitrogen and Phosphorus Removal in a Membrane Bioreactor. *Desalination* **2011**, 270 (1–3), 227–232.
- (51) Izadi, P.; Izadi, P.; Eldyasti, A. Understanding Microbial Shift of Enhanced Biological Phosphorus Removal Process (EBPR) under Different Dissolved Oxygen (DO) Concentrations and Hydraulic Retention Time (HRTs). *Biochem. Eng. J.* 2021, *166*, 107833.
- (52) Sena, M.; Rodriguez Morris, M.; Seib, M.; Hicks, A. An Exploration of Economic Valuation of Phosphorus in the Environment and Its Implications in Decision Making for Resource Recovery. *Water Res.* **2020**, *172*, 172.

- (53) Morelli, B.; Hawkins, T. R.; Niblick, B.; Henderson, A. D.; Golden, H. E.; Compton, J. E.; Cooter, E. J.; Bare, J. C. Critical Review of Eutrophication Models for Life Cycle Assessment. *Environ. Sci. Technol.* **2018**, *52* (17), 9562–9578.
- (54) Helmes, R. J. K.; Huijbregts, M. A. J.; Henderson, A. D.; Jolliet, O. Spatially Explicit Fate Factors of Phosphorous Emissions to Freshwater at the Global Scale. *Int. J. Life Cycle Assess.* **2012**, *17* (5), 646–654.